

12,16

## X-ray Study and Computer Simulation of the Structure of Amorphous-Crystalline Titanite

© O.V. Sidorova<sup>1</sup>, L.A. Aleshina<sup>1</sup>, A.D. Fofanov<sup>2</sup>

<sup>1</sup> Department of Solid State Physics, Petrozavodsk State University, Petrozavodsk, Republic of Karelia, Russian Federation

<sup>2</sup> Karelian Research Centre at Russian Academy of Sciences, Petrozavodsk, Republic of Karelia, Russian Federation

E-mail: solvak@petsru.ru

Received September 2, 2021

Revised September 21, 2021

Accepted September 21, 2021

The structure of amorphous-crystalline titanite obtained by mechanical activation was studied by X-ray diffraction and simulation methods. The short-range order characteristics were calculated using Finbak–Warren’s method. It was found that the coordination numbers of metal atoms decreased as the result of titanite grinding. The atomic configurations of short-range order of ground titanite were constructed by translation of titanite unit cell. The theoretical X-ray patterns were calculated using Debye’s method and were compared with the experimental curves. The structure of ground titanite in the mill with centrifugal factor 40g was described satisfactorily by the model of mechanical mixture of clusters containing 2016 atoms, disordered during the molecular dynamics with clusters containing 12096 atoms. The increase of grinding intensity led to the sharp decrease of sizes of small cluster.

**Keywords:** amorphous-crystalline titanite, X-ray diffraction, computer simulation, mechanical activation, Debye’s method.

DOI: 10.21883/PSS.2022.02.53274.197

### 1. Introduction

Titanite powders are extensively used in the construction industry as pigments [1,2]. Ultrafine mechanical grinding of CaTiSiO<sub>5</sub> is the basis of technology for production of fillers. It is known that the optical properties of titanite powders change during grinding [1]. In this case, the specific surface increases 30–50 times and its reactivity also increases [1–9]. Recently, titanite has attracted attention as biomedical material because of its high chemical stability [5]. Amorphization of the surface layer leads to titanite effectively absorbing both organic and inorganic substances. Functional materials (sorbents, pigments) can be obtained using this effect [6,7].

The structural state of metamict titanites was investigated by T. Beirau [10–12] using synchrotron XRD and vibration (Raman and IR) spectroscopy. It was shown that radiation-induced damage led to the formation of partially amorphous titanite with coexisting aperiodic and defect-enriched crystal regions. Basically, the space group of radiation-damaged titanite was *C2/c*, but there were regions with the space group *P21/c*. Radiation damage led to an increase of unit cell volume and a decrease of the coordination of Ti atoms from six to five and/or four. The transformation from an octahedral to a pyramidal and/or tetrahedral arrangement of the surrounding oxygen atoms led to a decrease of the Ti–O bond length, so the bond strength was increased. The lowering of Ti coordination violates the Ti–O–Ti interchain bonds, which was accompanied by a displacement of Ca atoms [10–12].

The method of mechanical activation (MA) can change crystals’ characteristics. Different crystallite microstructures can be achieved by selecting between grinding modes and environments.

There is much scope for pair distribution functions (PDF) application, especially to describe the changes in atomic structure of solids during grinding [13]. The quantification of the degree of amorphicity in a mineral resulting from grinding is relevant to further technological process.

Previous similar studies [14] were performed for pseudowollastonite CaSiO<sub>3</sub>. In [14], the model of structure of a mechanically activated for 30 min. pseudowollastonite was represented by a cluster consisting of four pseudowollastonite unit cells disordered as the result of molecular dynamics experiment, one unit cell of vaterite (CaCO<sub>3</sub>), and one unit cell of quartz (SiO<sub>2</sub>).

In this paper, mechanical activation of titanite mineral (orthosilicate) in mills with different centrifugal factors (CF) in air and in carbon dioxide atmosphere was studied. The structural analysis of atoms arrangement in a short-range order region in the amorphous-crystalline titanite was provided by two approaches: wide-angle X-ray diffraction and computer simulation. In the previously published work [14], we examined the effect of mechanical activation on the structure of pseudowollastonite, which belongs to the class of ring silicates. In terms of fundamental science, present studies are of interest because titanite belongs to orthosilicates.

## 2. Samples and methods

### 2.1. Samples

Titanite powders (CaTiSiO<sub>5</sub>) were provided by the I.V. Tananaev Institute of Chemistry and Technology of Rare Elements and Mineral Raw Materials of the Russian Academy of Sciences Kola Science Center (Apatites). The crystalline titanite was synthesized by sintering of CaCO<sub>3</sub> (reagent grade), TiO<sub>2</sub> (reagent grade), and amorphous SiO<sub>2</sub> taken in stoichiometric proportions, at 1200°C for 10 hours.

The samples of titanite were mechanically activated in a centrifugal planetary mill AGO-2 [15] (CF of 40 g) in air and in CO<sub>2</sub> for 30 min. and in a planetary micro mill Pulverisette 7 (CF of 95 g) in air for 30 min. Steel balls of 5-mm diameter were used as milling bodies. The weight of titanite was 10 g resulting in the ball-to-powder weight ratio of 20:1. The grinding process was dry.

### 2.2. X-ray diffraction experiment and data processing

X-ray patterns of titanite powders were obtained in symmetric reflection geometry on a DRON 6.0 diffractometer ( $U = 40$  kV,  $I = 21$  mA) using CuK $\alpha$  radiation ( $\lambda = 1.54178$  Å, the angular range  $2\theta$  from 2 to 145° with 0.02° step in the region of the peaks and with 0.2° step in the region of the background) and MoK $\alpha$  radiation ( $\lambda = 0.7107$  Å,  $U = 37$  kV,  $I = 30$  mA, angular range  $2\theta$  from 2 to 70° with step 0.2° and the angular range  $2\theta$  from 70 to 145° with steps 0.5°). The diffraction patterns were recorded 5 times. X-ray pattern of the air was measured without a sample in the range  $2\theta$  from 2 to 145° with 1° step. The crystal monochromator of pyrolytic graphite was located in the primary beams.

Unit cell parameters for the initial and the crystalline components of the titanite mechanically activated for 30 min. were determined using a full-profile analysis. Refinement of the atomic structure of the samples was performed with MRJA software systems [16].

The methodology for processing experimental data, calculating PDF, and determining from them the coordination numbers, radii, and blurring of coordination spheres, was implemented in the software package which was designed at Department of Solid State Physics of Petrozavodsk State University [14,17–24]. It is described in detail and implemented in studies of a number of materials, in particular [14,22,24].

According to Warren [17–24], the  $D(r)$  curve may be presented as a sum of pair functions:

$$D(r) = \sum_{j=1}^N \sum_{i=1}^M \frac{N_{ij}}{r_{ij}} P'_{ij}(r), \quad (1)$$

where  $N$  is the number of coordination sphere;  $M$  is the number of atoms in the formula unit;  $N_{ij}$  is the coordination number or the number of atoms  $j$  on the  $i$ -th coordination

sphere with radius  $r_{ij}$ . The effective pair function  $P'_{ij}(r)$  is the convolution of a pair function  $P_{ij}(r)$  with a Gauss function  $G_{ij}(r)$ .

The pair function characterizes the electron density distribution of one separate pair of atoms. The effective pair function is

$$P'(i, j) = \int_0^{s_{\max}} f_i(s) f_j(s) \exp[-(\alpha^2 + \sigma_{ij}^2) s^2] g^{-2}(s) \times \sin(sr_{ij}) \sin(sr) ds, \quad (2)$$

where  $s = \frac{4\pi \sin \theta}{\lambda}$  is the length of the diffraction vector ( $s_{\max} = 16.86$  Å<sup>-1</sup> for MoK $\alpha$  radiation),  $\alpha$  is a coefficient of attenuation factor  $\exp[-(\alpha^2 + \sigma_{ij}^2)] s^2$ ,  $\sigma_{ij}$  is blurring of coordinate spheres,  $g(s) = \frac{\sum_j f_j(s)}{\sum_j z_j(s)}$  is the peaking factor, where  $Z_j$  is the atomic number of the  $j^{\text{th}}$  element.

The coordination numbers  $N_{ij}$  were calculated from the PDF by the least squares method (LSM) using singular values decomposition (SVD), while radii  $r_{ij}$  and blurring  $\sigma_{ij}$  of coordination spheres were estimated by the method of successive approximations [23–26].

The starting values of the coordination spheres radii  $r_{ij}$  were data for crystalline phases of titanite. The blurring  $\sigma_{ij}$  was changed gradually from zero to a finite value corresponding to a minimum difference between  $D(r)$  and  $D_{\text{LSM}}(r)$ .  $D_{\text{LSM}}(r)$  curves were obtained by Eq. (1) for each set of  $r_{ij}$ ,  $\sigma_{ij}$ , and  $N_{ij}$  estimated by the LSM. The set of the obtained short-range order characteristics ( $N_{ij}$ ,  $r_{ij}$ , and  $\sigma_{ij}$ ) should be analyzed for reliability, and primarily by taking the crystal-chemical principle into consideration.

In multicomponent materials, different atoms may be located at interatomic distances of the same magnitude. In these cases, the resolution of  $D(r)$  calculated for non-crystalline materials is not sufficient for a separate calculation of the coordination numbers even when the SVD method is used. Therefore, to compare the experimental data with the corresponding values for the crystals, it was necessary to calculate the values of the radii and coordination numbers, combining the coordination spheres. In the case when spheres composing pairs of atoms of different types ( $i, j; i1, j1$ ) are combined, the coordination numbers for the crystals must be recalculated according to the relation  $N_{ij} = N_{i1, j1} \cdot \frac{Z_{i1} Z_{j1}}{Z_i Z_j}$ , which results from the equality of areas under the maxima of the PDF [23,24].

The discrepancy degree  $q$  of the experimental  $D(r)$  curve and  $D_{\text{LSM}}(r)$  curve was estimated as follows [23]:

$$q = \frac{\sum_{k=l_{\min}}^{l_{\max}} \frac{|D(r_k) - D_{\text{LSM}}(r_k)|}{D(r_k)}}{(l_{\max} - l_{\min}) + 1} \cdot 100\%, \quad (3)$$

where

$$\Delta D(r_k) = \sqrt{\frac{\sum_{m=1}^n [D_m(r_k) - \overline{D(r_k)}]^2}{n(n-1)}} \quad (4)$$

and

$$\overline{D(r_k)} = \frac{1}{n} \sum_{m=1}^n D_m(r_k). \quad (5)$$

The values of  $l_{\min}$  and  $l_{\max}$  limit the area of fitting of  $D_{\text{LSM}}(r)$  and  $D(r)$  by the values of  $r_{\min}$  and  $r_{\max}$ . That is,  $r_{\min}$  corresponds to the beginning of the first maximum, while  $r_{\max}$  is the radius of the last coordination sphere. In addition, the degree of coincidence of  $D_{\text{LSM}}(r)$  and  $D(r)$  was evaluated visually from the plot.

### 2.3. Methods of a structural model construction and theoretical X-ray patterns calculation

In order to describe three-dimensional atoms arrangement, the construction of clusters was performed in two ways. In the first case, the clusters were built by translation of a monoclinic unit cell of titanite phases along both the crystallographic directions ( $X, Y, Z$ ) and the Cartesian axes ( $x, y, z$ ). We varied the sizes of the clusters by changing the number of translations along the coordinate axes.

In the second case, monoclinic unit cells were shifted by the parallel displacements along each of three directions of the Cartesian axes ( $x, y, z$ ) relative to the first unit cell. The displacements were within the periods of the unit cell. The interatomic distances on the boundary between the unit cells were controlled.

Theoretical X-ray patterns of atoms configurations were calculated using modified Debye's formula [14,27–31]:

$$I(s) = \frac{1}{N_c} \left[ \sum_{i=1}^N f_i^2 + \sum_{i=1}^{N_{\max}} (f_{pi}^* f_{qi} + f_{pi} f_{qi}^*) \times N_{pqri} \frac{\sin(sr_i)}{(sr_i)} \exp(-0.5\varepsilon_i^2 s^2) \right], \quad (6)$$

where the first term in square brackets describes independent scattering of cluster atoms; the second term is due to the interference of the scattered waves;  $f_{pi}$ ,  $f_{qi}$  are the atomic scattering functions for the atoms pair of  $p$  and  $q$  sorts with the distance  $r_i$ ;  $N_{\max}$  is the number of different interatomic distances  $r_i$ ;  $\varepsilon_i$  is the variance of  $r_i$ ;  $N$  is the number of atoms;  $N_c$  is the number of composition units. Instead of summing over  $p$  and  $q$ , the expression in parentheses is multiplied by  $N_{pqri}$  (the number of atoms pairs of  $p$  and  $q$  sorts in the cluster that are at the same „average“ distance  $r_i$  from each other).

**Table 1.** Parameters  $A_{ij}$ ,  $\rho_{ij}$ , and  $C_{ij}$  of the Born–Mayer–Higgins semi-empirical interaction potential;  $q_i$  and  $q_j$  are the charges of ions of  $i$  and  $j$  types

| Ion–Ion                   | $A_{ij}$ , eV | $\rho_{ij}$ , Å | $C_{ij}$ , eV Å <sup>6</sup> | $q_i$ | $q_j$ |
|---------------------------|---------------|-----------------|------------------------------|-------|-------|
| Ca–O [33]                 | 1996.35       | 0.3189          | 26.57                        | +2    | –2    |
| Ti–O [34]                 | 2272.741      | 0.2986          | 0.0                          | +4    | –2    |
| Si–O [30] (orthosilicate) | 417.19        | 0.4297          | 0.0                          | +4    | –2    |
| O–O [35]                  | 15123.6       | 0.2230          | 28.43                        | –2    | –2    |

The reliability of the constructed models was assessed using a profile  $R$ -factor, which was calculated by the formula:

$$R_p = \frac{\sum_{i=1}^N |I_i^{\text{exp}} - I_i^{\text{calc}}|}{\sum_{i=1}^N I_i^{\text{exp}}}, \quad (7)$$

where  $I_i^{\text{exp}}$  and  $I_i^{\text{calc}}$  are the observed and the calculated values of the scattering intensity at each point of the X-ray pattern,  $N$  is the number of measurement points.

Two order-disturbance methods in the arrangement of cluster atoms were realized in this study. In the first case, the atoms of different sorts in the cluster were displaced at random from the initial positions within the range 0.1–0.2 Å.

Otherwise, the cluster was relaxed using molecular dynamics (MD) methods. MD experiments were conducted using the program designed at Department of Solid State Physics of Petrozavodsk State University (A.D. Fofanov, M.E. Prokhorskiy [32]). MD simulation of mechanically activated titanite was carried out in the canonical ensemble  $NVT$  ( $N$  is the number of particles,  $V$  is the volume, and  $T$  is absolute temperature). The calculation procedure is similar to that used in [14].

The used values of the parameters  $A_{ij}$ ,  $\rho_{ij}$ ,  $C_{ij}$  of the Born–Mayer–Higgins semi-empirical interaction potential are presented in Table 1.

The interactions of metal's ions with themselves and with the silicon were considered to be purely Coulombian, since there is no direct contact of the ions' electron shells in the structure.

The concentration of clusters of a certain type for the samples, in which the clusters with different sizes were observed, was calculated by the following formula:

$$C_f = \frac{\sum_j I_j^f(s_j) c_0 s_j^2}{\sum_j I_{\text{sum}}(s_j) s_j^2} \cdot 100\% \quad (8)$$

where  $I_j^f(s)$  is a scattering intensity of the cluster with  $f$  number normalized per unit of the composition;  $I_{\text{sum}}(s_j)$  is a total scattering intensity (sum of the scattering intensity of individual components);  $c_0$  is a contribution of the scattering intensity of the cluster to the total scattering

**Table 2.** The refined unit cell parameters for the crystalline component of the titanite samples

|              | $P2_1/a$ , initial crystalline titanite | MA for 30 min. in air (40 g) | MA for 30 min. in CO <sub>2</sub> (40 g) | MA for 30 min. in air (95 g) |
|--------------|---|------------------------------|--|------------------------------|
| $a$ , Å      | 7.055(2)                                | 7.057(8)                     | 7.057(7)                                 | 7.058(6)                     |
| $b$ , Å      | 8.715(2)                                | 8.717(1)                     | 8.718(9)                                 | 8.721(7)                     |
| $c$ , Å      | 6.559(6)                                | 6.551(8)                     | 6.556(7)                                 | 6.562(5)                     |
| $\beta$ , °  | 113.78(3)                               | 113.65(5)                    | 113.68(4)                                | 113.78(3)                    |
| $R_{wp}$ , % | 5.59                                    | 2.55                         | 2.25                                     | 4.19                         |
| $R_p$ , %    | 4.21                                    | 1.95                         | 1.59                                     | 3.26                         |

pattern. Summation was carried out across the region in which the experimental curve was registered.

The coordination numbers for the models were determined from function  $D(r)$  calculated by the formula:

$$D(r) = 2\pi^2 r \rho_e \cdot \sum_{j=1}^M Z_j + \int_0^{s_{\max}} H(s) \sin(sr) ds, \quad (9)$$

$$H(s) = s \cdot i(s) \exp(-\alpha^2 s^2) g^{-2}(s), \quad (10)$$

where  $s$ -weighted interference  $H(s)$  function and the interference function  $i(s)$  are obtained for the model;  $\rho_e$  is the average electron density of the material;  $\alpha$  is a coefficient of attenuation factor  $\exp(-\alpha^2 s^2)$ , which is usually equal to 0.1; the peaking factor  $g(s) = \frac{\sum_j f_j(s)}{\sum_j Z_j}$ , where  $Z_j$  is the atomic number of the  $j$ th element.

#### 2.4. Method of determining particles sizes (coherent scattering region) and microstrains values and crystallinity degree

The peak broadening analysis was performed by the method of Williamson and Hall [36]. The Cauchy and Gauss functions were used to determine particle sizes and microstrains [37,38]. In the first case, the width of the reflection  $\beta$  is related to the size of crystallites  $D$  and the value of microstrains  $\varepsilon$  by the ratio

$$\beta \cos \theta = \frac{\lambda}{D} + 4\varepsilon \sin \theta, \quad (11)$$

where  $\lambda$  is the wavelength of CuK $\alpha$  radiation,  $\theta$  is a diffraction angle.

In the second case, the size of crystallites  $D$  and the value of microstrains  $\varepsilon$  were determined from the ratio

$$(\beta \cos \theta)^2 = \left(\frac{\lambda}{D}\right)^2 + (4\varepsilon \sin \theta)^2. \quad (12)$$

The width  $\beta$  is the difference between the widths of XRD lines of the mechanically activated ( $w'$ ) and of the initial ( $w$ ) samples. The X-ray pattern of the initial non-deformed powder was used to account for the instrumental contribution. The values of  $\Delta D$  and  $\Delta \varepsilon$  were

calculated from errors in determining the width of the corresponding reflections in the X-ray diffraction patterns.

The crystallinity degree (CD) was calculated using the modified Ruland's method [39] as a ratio of the scattering intensity of the crystalline phase to the total scattering intensity of the crystalline and the amorphous phases according to Eq. (13):

$$CD = \left(\frac{I - I_{am}}{I}\right) \cdot 100\%, \quad (13)$$

where  $I$  is the total integrated scattering intensity of the crystalline and amorphous phases, calculated as the area under the entire experimental curve or selected for calculating the region of scattering angles  $2\theta$ :

$$I = \int_{2\theta_1}^{2\theta_2} I(2\theta) d(2\theta) \quad (14)$$

and  $I_{am}$  is integrated scattering intensity of the amorphous phase of the sample:

$$I_{am} = \int_{2\theta_1}^{2\theta_2} I_{am}(2\theta) d(2\theta). \quad (15)$$

## 3. Results and discussion

### 3.1. Structural characteristics of the crystalline component of the initial and mechanically activated for 30 min. titanite

The diffraction patterns of mechanically activated titanite showed that the samples had amorphous-crystalline structure (Fig. 1). Fig. 1 presents the results of the full-profile refinement of both the initial titanite and the crystalline components of mechanically activated (MA) samples.

It was established that the initial titanite structure and the crystalline phases of all MA samples correspond to the monoclinic syngony, space group  $P2_1/a$ . The refined parameters of the unit cell are shown in Table 2.

All parameters corresponded to the data for the initial powder within the error. Thus, mechanical activation for 30 min. did not lead to the unit cell deformation.

The particles size  $D$  and the values of strains are calculated orthogonal to diffraction planes (011) according

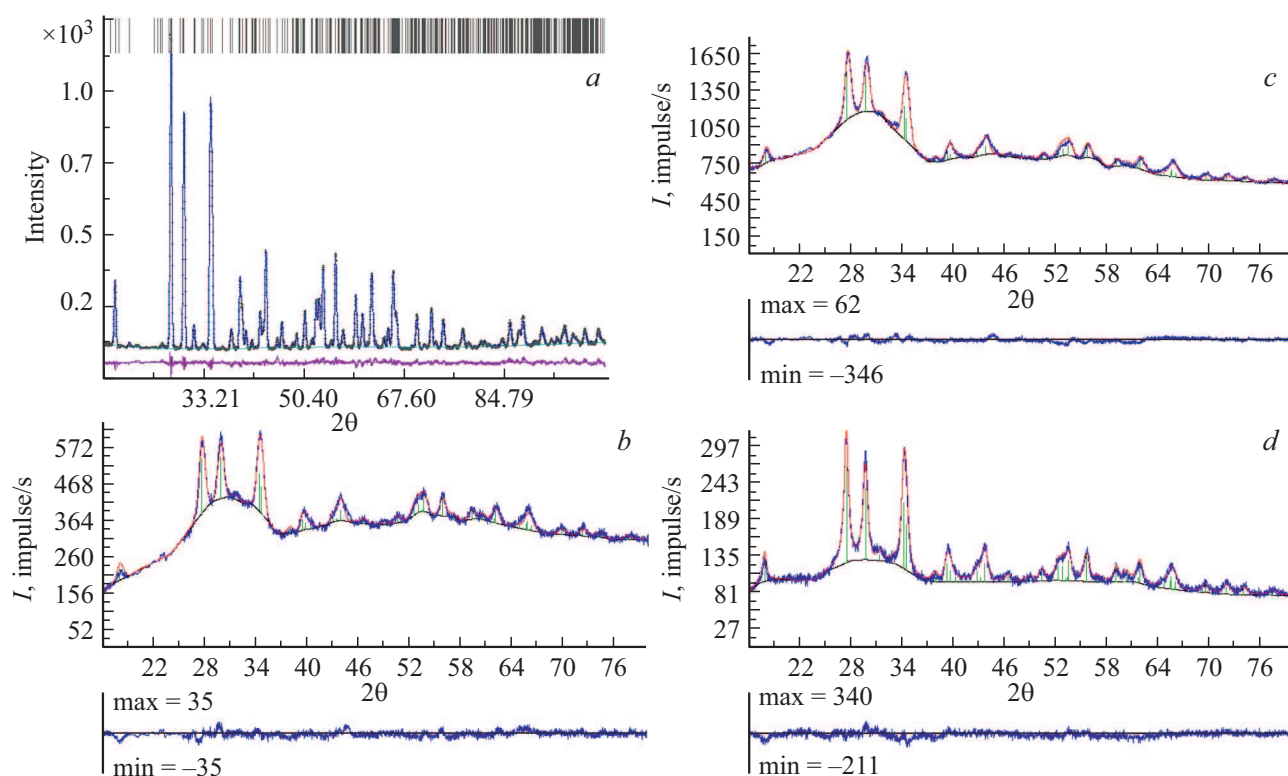


**Figure 1.** The X-ray diffraction patterns obtained in  $\text{CuK}\alpha$  radiation. Result of the full-profile refinement of *a*) initial titanite ( $R_p = 8.94\%$ ) and the crystalline components of mechanically activated (MA) samples: *b*) in air in AGO-2 ( $R_p = 2.55\%$ ); *c*) in  $\text{CO}_2$  in AGO-2 ( $R_p = 2.25\%$ ); *d*) in air in Pulverisette 7 ( $R_p = 4.19\%$ ). The bottom curves show the difference between the calculated and the experimental profiles.

to the Eq. (11), for the samples mechanically activated in air and in the atmosphere of carbon dioxide, and are given in Table 3.

Analysis of the peaks broadening on the XRD patterns of MA samples has shown that in mechanical activation, the reducing of particle size was more effective in the carbon dioxide than in the air atmosphere while the strains were higher.

When titanite was ground in the air and CF g was increased, the particle sizes were larger and microstrains were smaller (Table 3). It should be noted that the mechanical activation of pseudowollastonite for 30 min. at 40 g led to its complete amorphization [14].

**Table 3.** Particle sizes  $D$  ( $\Delta D = \pm 5 \text{ \AA}$ ) and microstrains  $\varepsilon$  ( $\Delta\varepsilon = 0.0001$ ) of titanite samples mechanically activated for 30 min.;  $hkl$  are indexes of reflections;  $2\theta$  is scattering angle

| $hkl$ | $2\theta, ^\circ$ | MA 30 min.       |               |                             |               |                  |               |
|-------|-------------------|------------------|---------------|-----------------------------|---------------|------------------|---------------|
|       |                   | in the air, 40 g |               | in the $\text{CO}_2$ , 40 g |               | in the air, 95 g |               |
|       |                   | $D, \text{ \AA}$ | $\varepsilon$ | $D, \text{ \AA}$            | $\varepsilon$ | $D, \text{ \AA}$ | $\varepsilon$ |
| 011   | 17.93             | 226              | 0.003         | 188                         | 0.003         | 330              | 0.0003        |
| 033   | 55.75             |                  |               |                             |               |                  |               |

### 3.2. Short-range order characteristics of mechanically activated titanite

The radii and blurring of coordination spheres and the coordination numbers were calculated using Finbak–Warren’s method from the curves, obtained in  $\text{MoK}\alpha$  radiations (Fig. 2). The intense diffuse maximum at  $s \sim 0.9 \text{ \AA}^{-1}$  (in the range of the scattering angles  $2\theta_{\text{MoK}\alpha} = 5.8^\circ$ ) was observed on the X-ray pattern of the titanite mechanically activated in the mill with CF of 40 g for 30 min. in both atmospheres (Fig. 2, *a*). The diffuse maximum in this range of the scattering angles did not increase with the CF increase to 95 g (Fig. 2, *a*). This maximum is usually associated with the correlation between the coherent scattering regions. The distance between regions centers was calculated from the position of the first maximum and equaled to  $7 \text{ \AA}$ .

The  $s$ -weighted interference function  $H(s)$  and pair functions  $D(r)$  are shown in Fig. 3. Despite the difference  $I(s)$  in the region of  $s \sim 1 \text{ \AA}^{-1}$  (Fig. 2), the PDF for the titanite samples mechanically activated for 30 min. in both mills differs slightly (Fig. 3).

The initial values of the radii of the coordination spheres were determined based on theoretical calculations for two polymorphs of titanite belonging to the monoclinic syngony. The phase of space group of symmetry  $P2_1/a$  is stable at room temperature and normal pressure [40–42]. Phase transition in the high-temperature

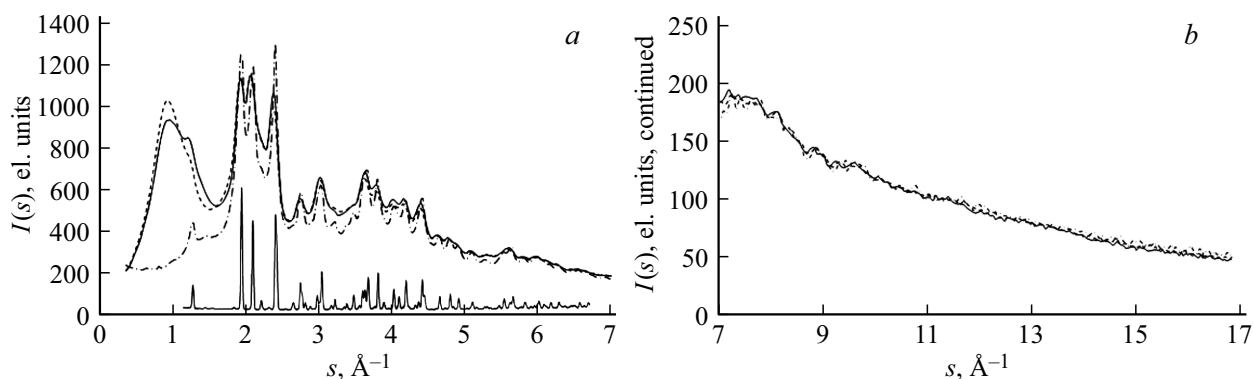


**Figure 2.** X-ray patterns obtained in MoK $\alpha$  radiation of crystalline (solid line, bottom part of the figure) titanite and the one mechanically activated for 30 min: solid line — in air in AGO-2, dashed line — in CO<sub>2</sub> in AGO-2, dash-and-dot line — in air in Pulverisette 7.

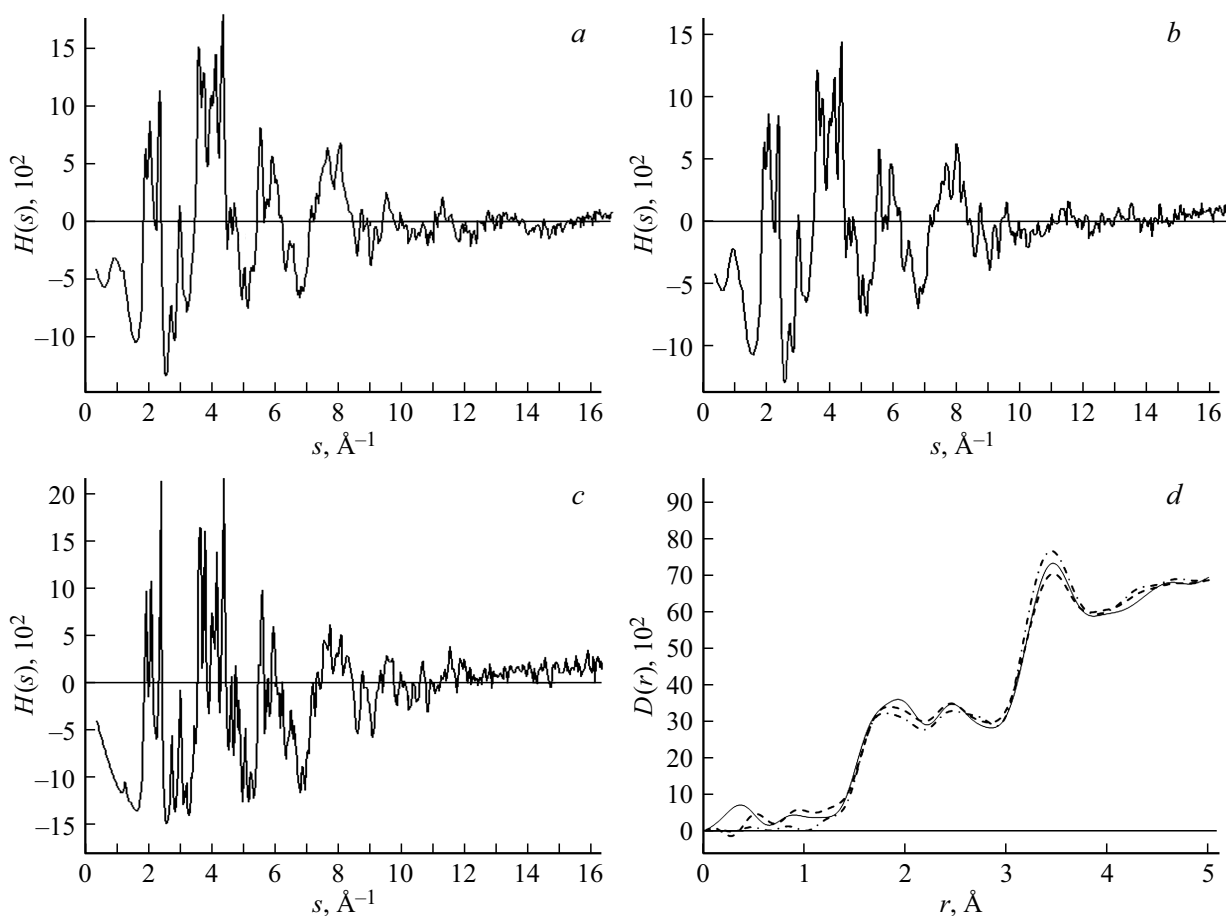


**Figure 3.** The  $s$ -weighted interference functions  $H(s)$ , AGO-2: *a*) in the air, *b*) in CO<sub>2</sub>, *c*) Pulverisette 7; *d*) pair functions  $D(r)$  for titanite mechanically activated for 30 min: solid line — in air in AGO-2, dashed line — in CO<sub>2</sub> in AGO-2, dash-and-dot line — in air in Pulverisette 7.

form with the space group of symmetry  $A2/a$  is caused at 270°C [40,42,43]. In both phases the tetrahedra of silicon are not connected with each other and interconnect with the chains of TiO<sub>6</sub> octahedra, forming a unified lattice (Fig. 4, *a*).

The calcium atoms are located in the voids of the lattice and surrounded by 7 oxygen atoms, forming a polyhedron of an irregular shape. The calcium polyhedra

are orientated along the  $c$  axis and arranged in the layers ordered checkerwise (Fig. 4, *b*). The titanium atoms are displaced from the geometric center of the octahedra in the low-temperature phase of symmetry  $P2_1/a$ . As a result, four Ti–O bonds have lengths from 1.984 to 2.025 Å, and two ones have lengths of 1.974 and 1.766 Å. The average radius of the first coordination sphere  $r_{\text{Ti-O}(1)}$  is 1.88 Å.

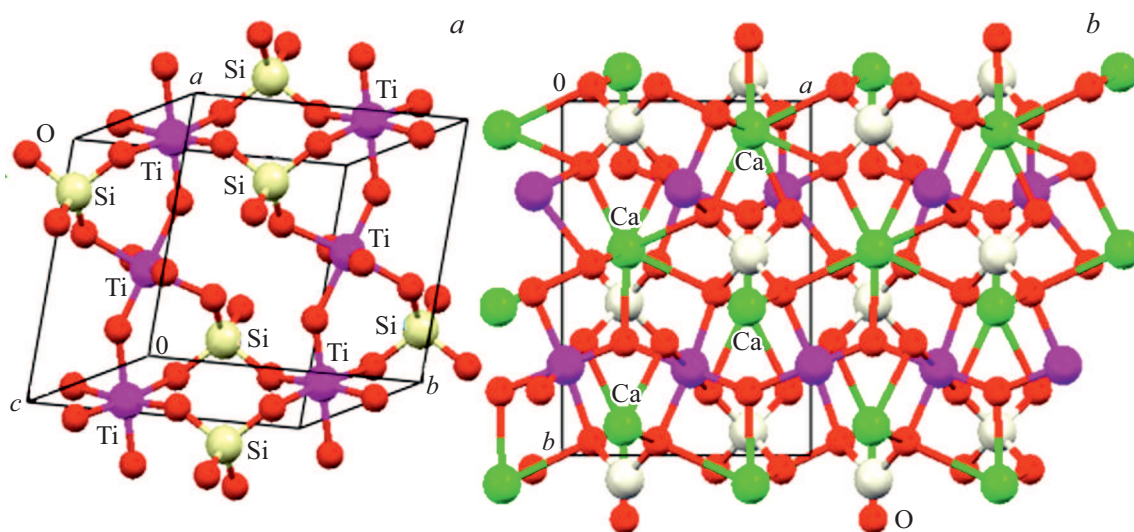


**Figure 4.** a) Bonds between octahedra  $\text{TiO}_6$  and tetrahedra  $\text{SiO}_4$ , b) arrangement of Ca atoms in the voids of the lattice of octahedra and tetrahedra, the projection onto the  $ab$  plane.

The form of the  $\text{TiO}_6$  octahedron is more regular in the  $A2/a$  phase. Titanium cations are displaced to the geometric center of the octahedron, so that the Ti–O distances are in pair equaled 1.867, 1.994, 2.016 Å. The average radius of the first coordination sphere  $r_{\text{Ti-O}(1)}$  is 1.95 Å. It is larger than in phase  $P2_1/a$ .

The first coordination spheres Ca–O(1), Si–O(1), Ti–O(1), O–O(1), the second coordination sphere of oxygen O–O(2), and the sphere of Ca–Si(1) in crystals have radii that differ significantly from each other. The coordination spheres of different types with larger radii may be similar. For example, Ca–O, Ti–Si, and Si–O spheres have similar radii ( $\sim 3.26$  Å, Table 4) and the coordination numbers of Ca–O and Si–O spheres were recalculated on Ti–Si(1) sphere (Table 4):

$$N'_{\text{Ti-Si}(1)} = N_{\text{Ca-O}} \cdot \frac{Z_{\text{Ca}}Z_{\text{O}}}{Z_{\text{Ti}}Z_{\text{Si}}} = 2 \cdot \frac{20 \cdot 8}{22 \cdot 14} = 1.039,$$

$$N''_{\text{Ti-Si}(1)} = N_{\text{Si-O}} \cdot \frac{Z_{\text{Si}}Z_{\text{O}}}{Z_{\text{Ti}}Z_{\text{Si}}} = 0.727,$$

$$\begin{aligned} N^*_{\text{Ti-Si}(1)} &= N'_{\text{Ti-Si}(1)} + N''_{\text{Ti-Si}(1)} + N'_{\text{Ti-Si}(1)} \\ &= 2 + 1.039 + 0.727 = 3.766. \end{aligned}$$

The details of this recalculation were described in [22,24,44].

The positions of the spheres are indicated by vertical lines on  $W(r)$  curves in Fig. 5.

The line heights for the different bonds correspond to the coordination number of sphere. Corresponding calculations from the experimental  $D(r)$  are presented in Table 5. As follows from Tables 4 and 5, the radii of the coordination spheres for two polymorphs of titanite differ significantly for the first sphere Ti–O(1) and for the last four spheres of Tables 4 and 5.

The average value of the interatomic distance Ti–O(1) for the sample mechanically activated for 30 min. in air

in both mills coincided in magnitude with the one for the high temperature phase of titanite ( $A2/a$ ), whereas it almost equaled to the value for the low-temperature phase ( $P2_1/a$ ) for the sample mechanically activated in  $\text{CO}_2$ .

Other radii calculated from the experiment for all MA samples corresponded to the values given for the  $P2_1/a$  phase. However, the coordination numbers differed markedly. The exception was the coordination of silicon ( $\text{SiO}_4$ ) which didn't change in the structure of mechanically activated samples. The number of oxygen neighbors around Ti and Ca atoms reduced during grinding. In case of the mechanical activation in the mill with CF of 95 g for 30 min., the number of oxygen neighbors around titanium atoms

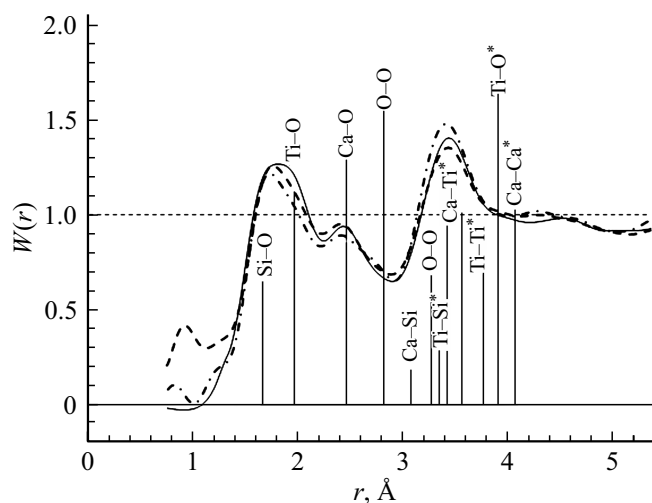


**Figure 5.** Pair correlation functions  $W(r)$  calculated from experiment for titanite mechanically activated for 30 min.: solid line — in air in AGO-2, dashed line — in  $\text{CO}_2$  in AGO-2, dash-and-dot line — in air in Pulverisette; \* shows the combined spheres.

**Table 4.** The radii of the coordination spheres  $r_{ij}$ , the coordination numbers  $N_{ij}$ , weighted average radii  $\langle r_{ij} \rangle$ , and summary coordination numbers  $N'_{ij}$  calculated for both titanite modifications [44]

| Titanite $P2_1/a$ |              |                  | Titanite $A2/a_{270^\circ C}$ |              |                  | Titanite $P2_1/a$ |                              |                   | Titanite $A2/a_{270^\circ C}$ |                              |                   |
|-------------------|--------------|------------------|-------------------------------|--------------|------------------|-------------------|------------------------------|-------------------|-------------------------------|------------------------------|-------------------|
|                   | $r_{ij}$ , Å | $N_{ij}$ , atoms |                               | $r_{ij}$ , Å | $N_{ij}$ , atoms |                   | $\langle r_{ij} \rangle$ , Å | $N'_{ij}$ , atoms |                               | $\langle r_{ij} \rangle$ , Å | $N'_{ij}$ , atoms |
| Si–O              | 1.64         | 4.0              | Si–O                          | 1.64         | 4.0              | Si–O(1)           | 1.64                         | 4.00              | Si–O(1)                       | 1.64                         | 4.00              |
| Ti–O              | 1.77         | 1.0              | Ti–O                          | 1.87         | 2.0              | Ti–O(1)           | 1.88                         | 6.00              | Ti–O(1)                       | 1.94                         | 6.00              |
| Ti–O              | 2.00         | 5.0              | Ti–O                          | 2.01         | 4.0              |                   |                              |                   |                               |                              |                   |
| Ca–O              | 2.27         | 1.0              | Ca–O                          | 2.29         | 1.0              | Ca–O(1)           | 2.44                         | 7.00              | Ca–O(1)                       | 2.44                         | 7.00              |
| Ca–O              | 2.41         | 4.0              | Ca–O                          | 2.41         | 4.0              |                   |                              |                   |                               |                              |                   |
| Ca–O              | 2.63         | 2.0              | Ca–O                          | 2.63         | 2.0              |                   |                              |                   |                               |                              |                   |
| O–O               | 2.60         | 0.8              | O–O                           | 2.63         | 1.2              | O–O(1)            | 2.80                         | 8.40              | O–O(1)                        | 2.81                         | 8.40              |
| O–O               | 2.74         | 7.0              | O–O                           | 2.72         | 3.6              |                   |                              |                   |                               |                              |                   |
| O–O               | 3.06         | 0.6              | O–O                           | 2.82         | 2.4              |                   |                              |                   |                               |                              |                   |
|                   |              |                  | O–O                           | 3.07         | 1.2              |                   |                              |                   |                               |                              |                   |
| Ca–Si             | 3.06         | 1.0              | Ca–Si                         | 3.07         | 1.0              | Ca–Si(1)          | 3.06                         | 1.00              | Ca–Si(1)                      | 3.07                         | 1.00              |
| Ca–O              | 3.22         | 2.0              | Ca–O                          | 3.22         | 2.0              | Ti–Si(1)          | 3.26                         | 3.77              | Ti–Si(1)                      | 3.26                         | 3.77              |
| Ti–Si             | 3.28         | 2.0              | Ti–Si                         | 3.28         | 2.0              |                   |                              |                   |                               |                              |                   |
| Si–O              | 3.29         | 2.0              | Si–O                          | 3.29         | 2.0              |                   |                              |                   |                               |                              |                   |
| O–O               | 3.33         | 1.4              | O–O                           | 3.32         | 1.2              | O–O(2)            | 3.33                         | 1.40              | O–O(2)                        | 3.38                         | 1.60              |
|                   |              |                  | O–O                           | 3.44         | 0.4              |                   |                              |                   |                               |                              |                   |
| Ca–Ti             | 3.38         | 4.0              | Ca–Ti                         | 3.38         | 4.0              | Ca–Ti(1)          | 3.41                         | 6.16              | Ca–Ti(1)                      | 3.41                         | 6.16              |
| Si–O              | 3.41         | 3.0              | Si–O                          | 3.41         | 3.0              |                   |                              |                   |                               |                              |                   |
| Ti–Si             | 3.43         | 2.0              | Ti–Si                         | 3.43         | 2.0              |                   |                              |                   |                               |                              |                   |
| Ca–Si             | 3.53         | 4.0              | Ca–Si                         | 3.53         | 4.0              | Ti–Ti(1)          | 3.55                         | 5.70              | Ti–Ti(1)                      | 3.55                         | 5.81              |
| Ti–Ti             | 3.53         | 2.0              | Ti–Ti                         | 3.53         | 2.0              |                   |                              |                   |                               |                              |                   |
| Ti–O              | 3.49         | 1.0              | Ti–O                          | 3.55         | 2.0              | Ti–O(2)           | 3.75                         | 5.34              | Ti–O(2)                       | 3.79                         | 7.27              |
| Ca–O              | 3.58         | 2.0              | Ca–O                          | 3.58         | 2.0              |                   |                              |                   |                               |                              |                   |
| Ti–O              | 3.60         | 1.0              | O–O                           | 3.57         | 0.8              |                   |                              |                   |                               |                              |                   |
| O–O               | 3.69         | 2.2              | O–O                           | 3.75         | 2.0              |                   |                              |                   |                               |                              |                   |
| Si–O              | 3.77         | 4.0              | Si–O                          | 3.77         | 4.0              | Ti–O(3)           | 3.89                         | 8.86              | Ti–O(3)                       | 3.91                         | 7.86              |
| Ti–O              | 3.78         | 2.0              | Ti–O                          | 3.86         | 4.0              |                   |                              |                   |                               |                              |                   |
| Ca–O              | 3.86         | 4.0              | Ca–O                          | 3.86         | 4.0              |                   |                              |                   |                               |                              |                   |
| Si–Si             | 3.91         | 2.0              | Si–Si                         | 3.91         | 2.0              | Ca–Ca(1)          | 4.06                         | 5.57              | Ca–Ca(1)                      | 4.09                         | 4.82              |
| Ti–O              | 3.92         | 3.0              | Ti–O                          | 3.95         | 2.0              |                   |                              |                   |                               |                              |                   |
| Ca–Ca             | 3.99         | 2.0              | Ca–Ca                         | 3.99         | 2.0              | O–O               |                              |                   |                               |                              |                   |
| O–O               | 4.00         | 0.8              | O–O                           | 4.01         | 0.8              |                   |                              |                   |                               |                              |                   |
|                   |              |                  | O–O                           | 4.17         | 0.8              | Ti–O              |                              |                   |                               |                              |                   |
| Ti–O              | 4.09         | 4.0              | Ti–O                          | 4.11         | 2.0              |                   |                              |                   |                               |                              |                   |
| Si–O              | 4.16         | 6.0              | Si–O                          | 4.16         | 6.0              |                   |                              |                   |                               |                              |                   |

**Table 5.** The radii ( $\Delta r_{ij} = \pm 0.01 \text{ \AA}$ ) and blurring  $\sigma_{ij}$  ( $\Delta \sigma_{ij} = \pm 0.2 \text{ \AA}$ ) of the coordination spheres and the coordination numbers for the ground titanite samples and the corresponding data for the crystal

| Type of sphere                                     | MA in the air, 30 min. (40 g)<br>[41] |                     |                  | MA in CO <sub>2</sub> , 30 min. (40 g)<br>[41] |                     |                  | MA in the air, 30 min. (95 g) |                     |                  | $P2_1/a/A2/a$                  |                  |
|--|---------------------------------------|---------------------|------------------|--|---------------------|------------------|-------------------------------|---------------------|------------------|--------------------------------|------------------|
|  | $r_{ij}$ , \AA                        | $\sigma_{ij}$ , \AA | $N_{ij}$ , atoms | $r_{ij}$ , \AA                                 | $\sigma_{ij}$ , \AA | $N_{ij}$ , atoms | $r_{ij}$ , \AA                | $\sigma_{ij}$ , \AA | $N_{ij}$ , atoms | $\langle r_{ij} \rangle$ , \AA | $N_{ij}$ , atoms |
| Si–O(1)  | 1.64                                  | 0.18                | $3.94 \pm 0.02$  | 1.67   | 0.27                | $3.99 \pm 0.02$  | 1.64                          | 0.23                | $3.93 \pm 0.04$  | 1.64                           | 4.00             |
| Ti–O(1)  | 1.95                                  | 0.25                | $5.76 \pm 0.05$  | 1.90   | 0.25                | $5.55 \pm 0.05$  | 1.95                          | 0.28                | $4.50 \pm 0.05$  | 1.88/1.94                      | 6.00             |
| Ca–O(1)  | 2.44                                  | 0.19                | $5.59 \pm 0.02$  | 2.44   | 0.17                | $6.84 \pm 0.12$  | 2.44                          | 0.30                | $6.85 \pm 0.06$  | 2.44                           | 7.00             |
| O–O(1)   | 2.80                                  | 0.20                | $7.12 \pm 0.04$  | 2.80   | 0.17                | $6.41 \pm 0.06$  | 2.80                          | 0.20                | $6.62 \pm 0.08$  | 2.80                           | 8.40             |
| Ca–Si(1)   | 3.06                                  | 0.20                | $0.92 \pm 0.10$  | 3.00   | 0.02                | $1.20 \pm 0.24$  | 3.06                          | 0.11                | $0.94 \pm 0.05$  | 3.06                           | 1.00             |
| O–O(2)   | 3.33                                  | 0.17                | $1.32 \pm 0.45$  | 3.32   | 0.01                | $1.88 \pm 0.41$  | 3.31                          | 0.01                | $1.47 \pm 0.07$  | 3.33                           | 1.40             |
| Data, calculated for combined coordination spheres |                                       |                     |                  |  |                     |                  |                               |                     |                  |                                |                  |
| Ti–Si(1)   | 3.26                                  | 0.20                | $3.16 \pm 0.17$  | 3.25   | 0.08                | $2.10 \pm 0.15$  | 3.23                          | 0.22                | $3.61 \pm 0.20$  | 3.26                           | 3.77             |
| Ca–Ti(1)   | 3.41                                  | 0.24                | $3.70 \pm 0.34$  | 3.41   | 0.27                | $5.09 \pm 0.64$  | 3.41                          | 0.25                | $3.77 \pm 0.32$  | 3.41                           | 6.16             |
| Ti–Ti(1)   | 3.55                                  | 0.13                | $10.11 \pm 1.24$ | 3.56   | 0.01                | $7.59 \pm 0.75$  | 3.55                          | 0.08                | $7.76 \pm 0.57$  | 3.55                           | 5.70/5.81        |
| Ti–O(2)  | 3.75                                  | 0.15                | $7.60 \pm 0.87$  | 3.75   | 0.15                | $7.67 \pm 0.87$  | 3.76                          | 0.15                | $7.53 \pm 0.86$  | 3.75/3.79                      | 5.34/7.27        |
| Ti–O(3)  | 3.89                                  | 0.20                | $3.89 \pm 0.66$  | 3.89   | 0.11                | $7.81 \pm 0.46$  | 3.89                          | 0.15                | $9.51 \pm 1.33$  | 3.89/3.91                      | 8.86/7.86        |
| Ca–Ca(1)   | 4.06                                  | 0.20                | $12.83 \pm 0.18$ | 4.06   | 0.07                | $7.48 \pm 0.86$  | 4.06                          | 0.12                | $6.78 \pm 0.75$  | 4.06/4.09                      | 5.57/4.82        |

decreased by 1.5 (Table 5). Similar results were observed in the studies of radiation damaged titanite [10–12]. The number of oxygen neighbors of calcium atoms sharply decreased only after grinding in air in the mill with CF of 40 g (Table 5). As a consequence, the coordination number of  $N_{O-O(1)}$  of the mechanically activated samples became lower than the one in crystal modification.

Thus, mechanical activation in air for 30 min. in both mills led to the difference between the distributions of atoms over the coordination spheres for these samples. The obtained  $r_{ij}$  and  $N_{ij}$  differed from these for both crystal modifications. In the samples mechanically activated in CO<sub>2</sub>, the atoms distribution over the coordination spheres basically corresponded to the data calculated for the low-temperature phase of the titanite with space group  $P2_1/a$ .

### 3.3. Analysis of atoms arrangement in short-range order region by modeling XRD patterns

#### 3.3.1. Titanite mechanically activated at 40 g for 30 min.

Scattering intensity  $I(s)$  and  $s$ -weighted interference function were calculated using modified Debye's formula [14,27–31] for one unit cell and for the clusters obtained by the translation of unit cells of both titanite modifications (with space groups  $P2_1/a$  and  $A2/a$ ). We considered the clusters consisting of various number of unit cells.

For the titanite mechanically activated for 30 min. in the mill with CF of 40 g, the intensity calculated for the clusters with sizes  $1a \times 3b \times 4c$  (1, 3, and 4 are the numbers of translations along corresponding crystallographic axes of unit cell with group symmetry  $P2_1/a$ ) were closer to the experimental ones (Fig. 6, *a* and *b*). The cluster contained 384 atoms: 48 of Ca, 48 of Ti, 48 of Si, and 240 of O. Construction of the clusters was performed in two ways, described in Section 2.2. The cluster built using the first method is presented in Fig. 6, *c*. As per the second method, the unit cell was shifted by the parallel transport along the Cartesian  $z$ -axis to 6.6 \AA and along the Cartesian  $y$ -axis to 8.72 \AA relative to the first unit cell (the given distances were within the periods of unit cells of both titanite crystalline modification with space groups  $P2_1/a$  and  $A2/a$ ) (Fig. 6, *d*).

Fig. 6 shows that the difference in the construction method of the cluster led to a distinction in the shape of the  $I(s)$  curve in the field of  $s = 0.9 \text{ \AA}^{-1}$  ( $2\theta \sim 5.8^\circ$ ). In case of the cluster obtained by translation of unit cell along the crystallographic axes ( $X, Y, Z$ ), this diffuse maximum did not occur on the theoretical  $I(s)$  curve. The profile  $R$ -factor in both cases amounted to  $R_p = 16\%$ .

Disordering of the cluster of the above-mentioned size with the MD method did not improve the coincidence with the experiment. Thereby, the clusters of various sizes and forms were constructed using both methods for the phases of both  $P2_1/a$  and  $A2/a$  and were relaxed using the MD method. The calculated  $I(s)$  and  $H(s)$  curves matched

**Table 6.** The radii ( $\Delta r_{ij} = \pm 0.02 \text{ \AA}$ ) and blurring  $\sigma_{ij}$  ( $\Delta \sigma_{ij} = \pm 0.1 \text{ \AA}$ ) of the coordination spheres and the coordination numbers for the ground titanite samples and the corresponding data for the model of mechanical mixture consisting of the clusters of both  $3a \times 3b \times 7c$  and  $6a \times 9b \times 7c$

| Type of sphere | MA in the air, 30 min. (40 g)<br>[41] |                              |                  | Mechanical mixture consisting<br>of the clusters $3a \times 3b \times 7c$ and $6a \times 9b \times 7c$ |                              |                  | $P2_1/a/A2/a$                           |                  |
|----------------|---------------------------------------|------------------------------|------------------|--|------------------------------|------------------|---|------------------|
|                | $r_{ij}$ , $\text{\AA}$               | $\sigma_{ij}$ , $\text{\AA}$ | $N_{ij}$ , atoms | $r_{ij}$ , $\text{\AA}$  | $\sigma_{ij}$ , $\text{\AA}$ | $N_{ij}$ , atoms | $\langle r_{ij} \rangle$ , $\text{\AA}$ | $N_{ij}$ , atoms |
| Si–O(1)        | 1.64                                  | 0.18                         | $3.94 \pm 0.02$  | 1.64   | 0.14                         | $3.97 \pm 0.03$  | 1.64                                    | 4.00             |
| Ti–O(1)        | 1.95                                  | 0.25                         | $5.76 \pm 0.05$  | 1.93   | 0.10                         | $4.75 \pm 0.05$  | 1.88/1.94                               | 6.00             |
| Ca–O(1)        | 2.44                                  | 0.19                         | $5.59 \pm 0.02$  | 2.44   | 0.28                         | $6.81 \pm 0.05$  | 2.44                                    | 7.00             |
| O–O(1)         | 2.80                                  | 0.20                         | $7.12 \pm 0.04$  | 2.78   | 0.17                         | $6.15 \pm 0.06$  | 2.80                                    | 8.40             |
| Ca–Si(1)       | 3.06                                  | 0.20                         | $0.92 \pm 0.10$  | 3.00   | 0.01                         | $0.18 \pm 0.10$  | 3.06                                    | 1.00             |
| O–O(2)         | 3.33                                  | 0.17                         | $1.32 \pm 0.45$  | 3.2  | 0.01                         | $3.11 \pm 0.16$  | 3.33                                    | 1.40             |

with the experimental ones in case of the cluster with size  $3a \times 3b \times 7c$  obtained by the translation of unit cell in phase  $A2/a$  along the crystallographic axes ( $X, Y, Z$ ) and relaxed by the MD method (Fig. 7, *a* and *b*, Fig. 8). The profile  $R$ -factor was 13%.  $R_p$  was 9% when the maximum at  $s = 0.95 \text{ \AA}^{-1}$  on the experimental curve was excluded from the calculation.

The atomic structure of the cluster before and after MD experiment is shown in Fig. 8.

The cluster analysis showed that the  $\text{TiO}_6$  octahedra chains are present in the configuration that was disordered by the MD method. However, the coordination of Ti atom decreased. Specifically, 131 of 253 Ti atoms were surrounded by five oxygen atoms, 80 atoms of Ti had the coordination equal to 6. There were Ti atoms with the coordination of 4 and 3 on the cluster surface. This result was consistent with the calculation of the coordination numbers obtained using Finbak's method (Table 4). The coordination of Ca atoms in the cluster disordered by MD equaled to 3–12.6% (32 of Ca atoms), 4–22.9% (58 of Ca atoms), 5–24.5% (62 of Ca atoms) 6–18.6% (47 of Ca atoms), 7–15.4% (39 of Ca atoms).

However, the broad diffuse maximum at  $s = 0.9 \text{ \AA}^{-1}$  did not occur and the narrow diffraction peak ( $s = 2.375 \text{ \AA}^{-1}$ ) belonging to crystalline phase was not described in this model. The degree of crystallinity calculated from experimental XRD pattern according to Eq. (13) was 37%. The sizes of coherent scattering regions were calculated for all peaks on XRD pattern of titanite according of Sherrer's formula [45] and were in the range from 26 to 80  $\text{\AA}$ . The error in the sizes of coherent scattering regions was 5  $\text{\AA}$ .

We varied the sizes of the cluster of the crystalline component within these limits. The number of translations ( $a, b, c$ ) was ranged from 1 to 10 for the crystallographic axes ( $X, Y$ , and  $Z$ ). Within these limits, all possible translations combinations were considered.

It was found that the best match between the experimental and calculated curves was obtained in the case of mechanical mixture of the cluster of  $3a \times 3b \times 7c$  disordered by MD and clusters of  $6a \times 9b \times 7c$  size describing the scattering of the amorphous and crystalline phases.

The final theoretical scattering intensity  $I(s)$  was calculated by adding 0.8 of scattering intensity of the cluster with sizes  $3a \times 3b \times 7c$  (21; 26; 46  $\text{\AA}$  (2016 atoms)) disordered

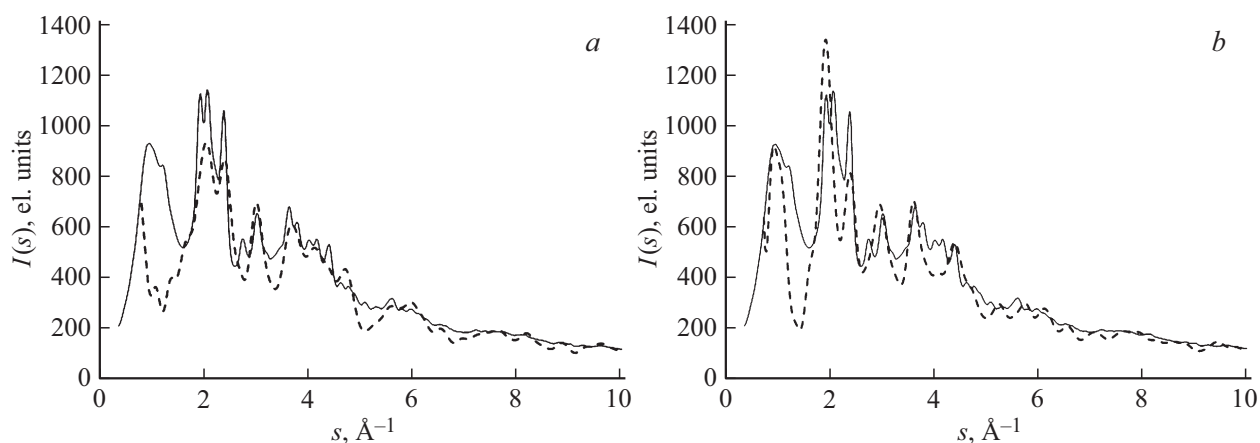


**Figure 6.** XRD patterns, the experimental (solid line) and the calculated (dashed line) ones for the clusters with sizes of  $1a \times 3b \times 4c$  and atoms arrangement in them at two different orientations in the space: *a*) and *c*) the first method of construction; *b*) and *d*) the second method of construction.

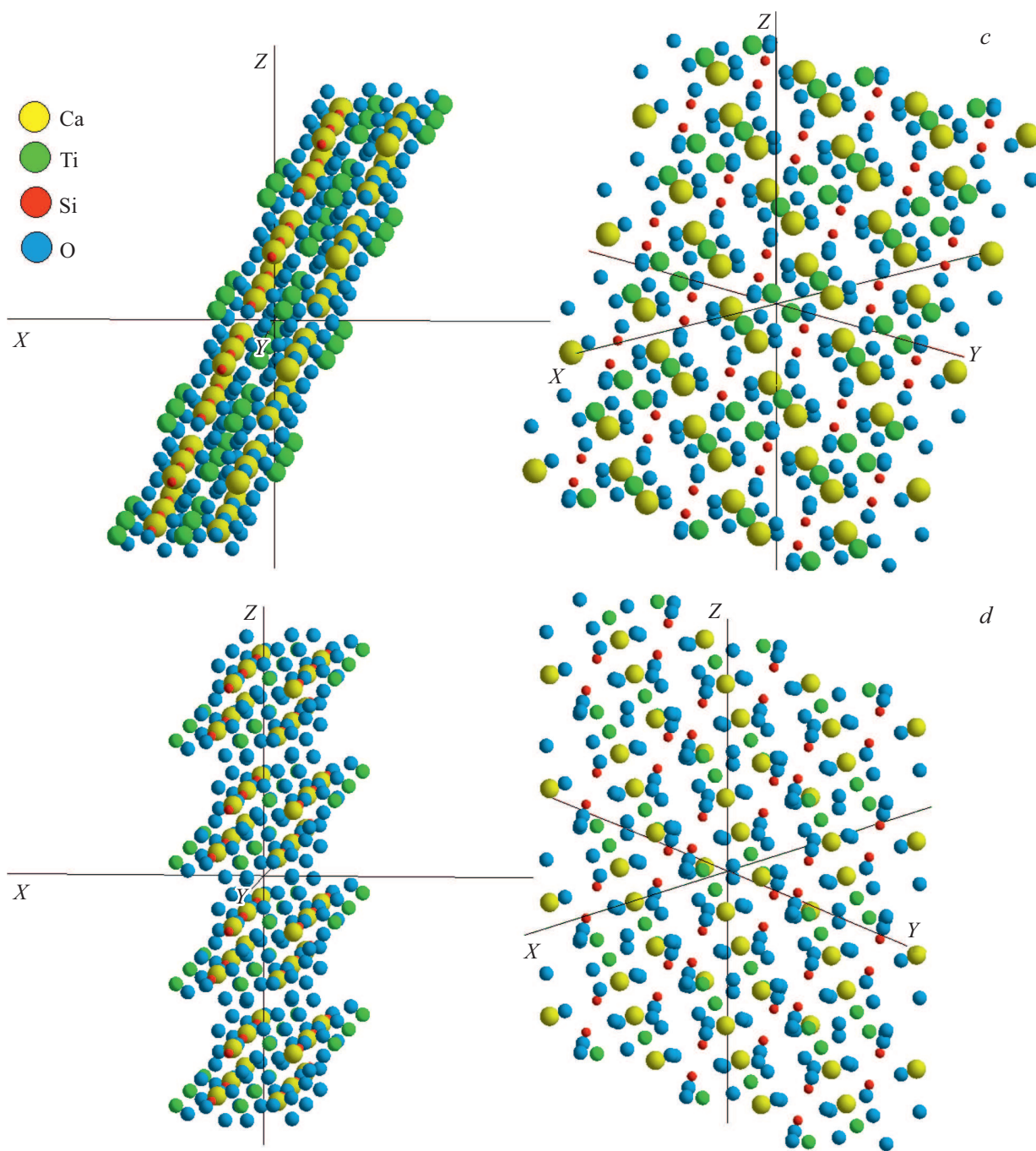


Figure 6 (continued).

by MD experiment and by adding 0.2 of scattering intensity of the cluster with sizes  $6a \times 9b \times 7c$  (59.5; 78; 41 Å (12096 atoms)) (Fig. 7, c). The values of phase concentrations calculated for the model were 80 and 20%.

Calculations of the coordination spheres radii and the coordination numbers from the experimental  $D(r)$  (Fig. 9) and for the model of mechanical mixture consisting of the clusters  $3a \times 3b \times 7c$  and  $6a \times 9b \times 7c$  are presented in Table 6.

The analysis of Table 6 showed that the data calculated for the model were close to the experimental data. The

curves differ due to blurring the maxima while keeping the same area under themselves. It means that the blurring is caused by a higher dispersion of interatomic distances in the sample compared to that in the model.

Thus, the structure of the titanite mechanically activated for 30 min. in the mill with CF of 40 g (AGO-2) is satisfactorily described by the mechanical mixture of randomly disoriented clusters with size of  $6a \times 9b \times 7c$  and one with linear size of  $3a \times 3b \times 7c$  (2016 atoms) constructed by the translation along the crystallographic axes ( $X, Y, Z$ ) and disordered as a result of the MD experiment.

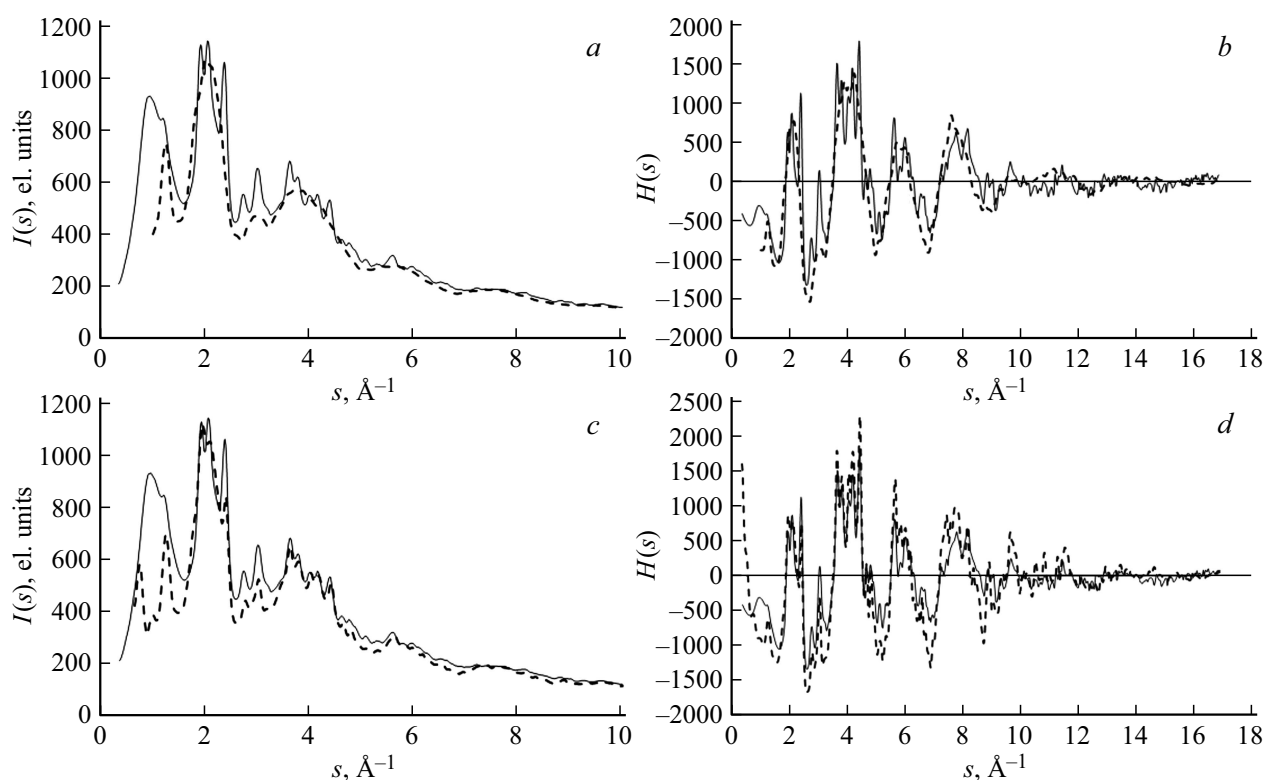


**Figure 7.** XRD patterns and  $s$ -weighted interference functions  $H(s)$ : experimental (solid line) and calculated (dashed line). *a*) and *b*): for the cluster of  $3a \times 3b \times 7c$  (21; 26; 46  $\text{\AA}$ , monoclinicity angle  $114^\circ$ , 2016 atoms,  $R_p = 13\%$ ; *c*) and *d*): for the mechanical mixtures of the cluster of  $3a \times 3b \times 7c$  disordered in MD experiment and cluster of  $6a \times 9b \times 7c$ ,  $R_p = 11\%$ .

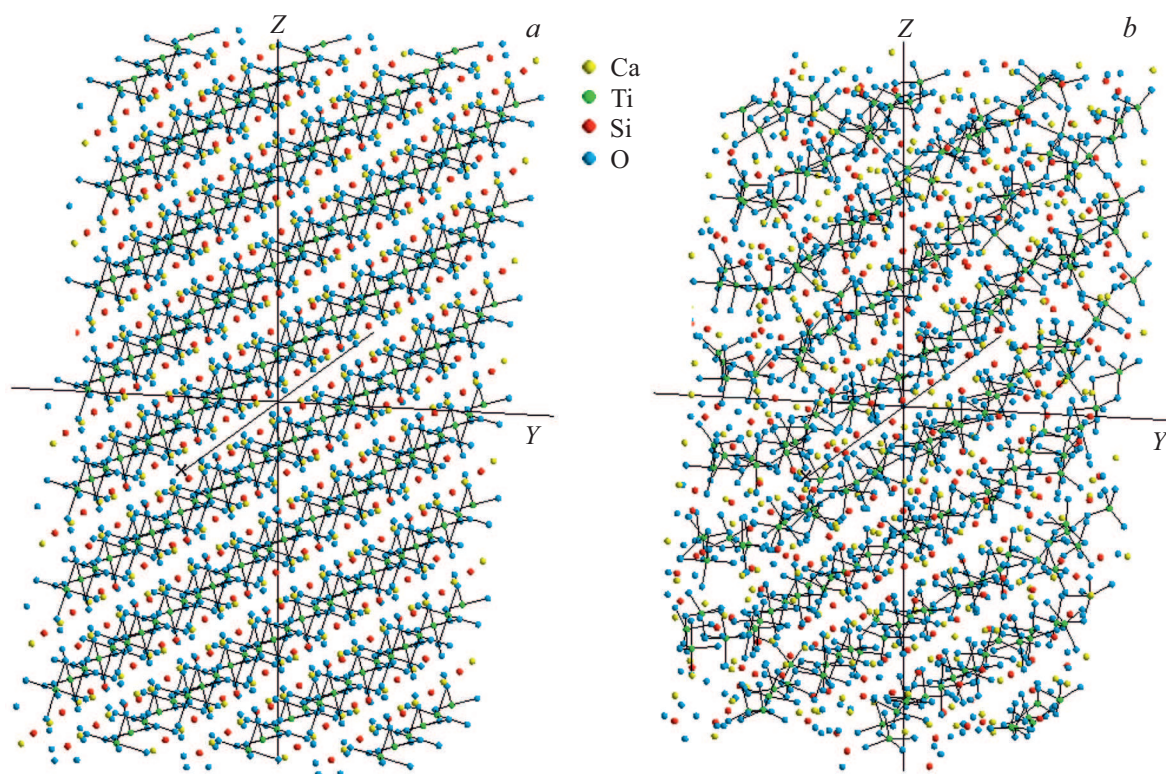


**Figure 8.** Cluster of  $3a \times 3b \times 7c$ : *a*) before MD; *b*) after 50000 steps of MD. Ti–O bonds are presented.

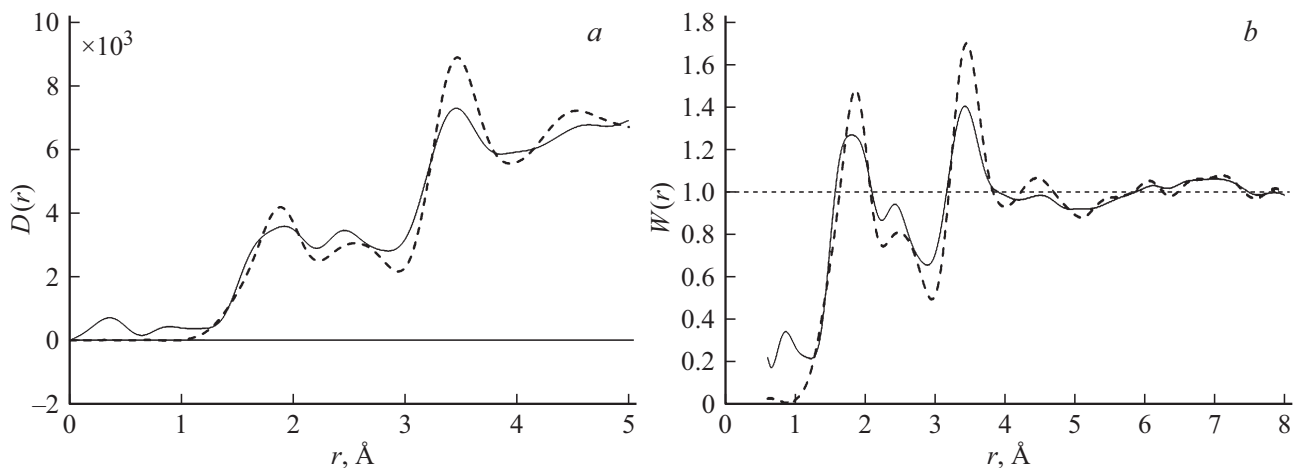


**Figure 9.** *a)* Pair functions  $D(r)$  and *b)* pair correlation function  $W(r)$  for titanite mechanically activated for 30 min. in AGO, calculated from experiment (solid line) and for the model (dashed line) of mechanical mixture consisting of the clusters of  $3a \times 3b \times 7c$  disordered by MD and the clusters of  $6a \times 9b \times 7c$ .

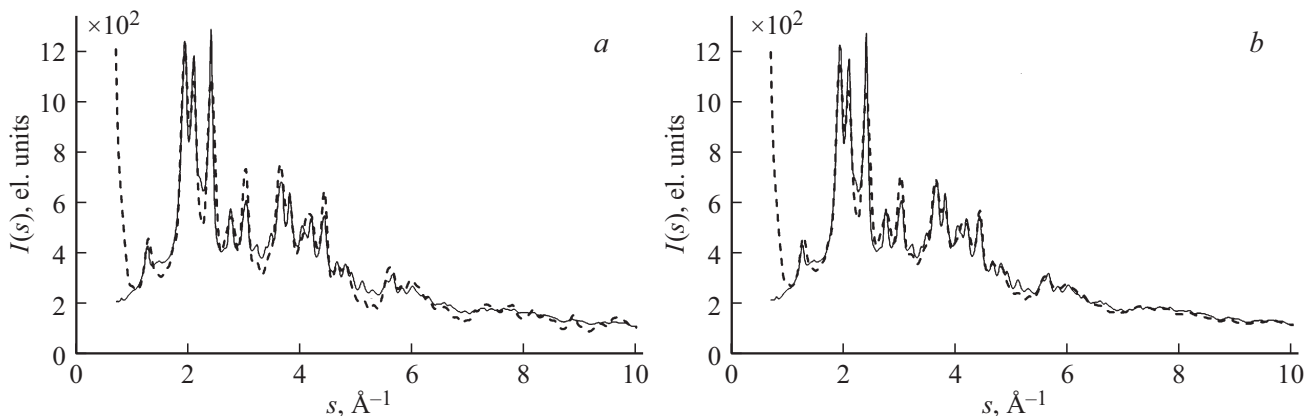


**Figure 10.** Scattering intensity, experimental (solid line) and calculated (dashed line) for the mechanical mixtures of the clusters: *a)*  $1a \times 1b \times 2c$  and  $5a \times 4b \times 10c$ ,  $R_p = 9.6\%$ ; *b)*  $1a \times 1b \times 2c$  cluster and the disordered one of  $5a \times 4b \times 10c$ ,  $R_p = 6.9\%$ .

The maximum in the region  $s = 0.9 \text{ \AA}^{-1}$  occurred at the theoretically calculated intensity only for the model, which is a set of randomly disoriented clusters with  $1a \times 3b \times 4c$  size, constructed by shifting unit cell with  $P2_1/a$  symmetry along the Cartesian axes ( $x, y, z$ ). This cluster consists of 384 atoms: 48 of Ca, 48 of Ti, 48 of Si, and 240 of O.

As there was not the full amorphization of titanite during mechanical activation for 30 min. at 40 g, the centrifugal factor was increased.

### 3.3.2. Titanite mechanically activated in the mill with CF of 95 g for 30 min.

To describe the structure of the titanite mechanically activated in the mill with CF of 95 g for the same time (30 min.), the clusters of different sizes were constructed by the translation of unit cells of both modifications along the crystallographic axes ( $X, Y, Z$ ). The variations were performed within the same limits as mentioned above for CF of 40 g. The sizes of coherent scattering regions

calculated according to the Sherrer's formula [45] were from 60 to 80 Å for the crystalline component and up to 13 Å for the amorphous component. The error in the sizes of coherent scattering regions was 5 Å.

The scattering pattern calculated for the mechanical mixture of the clusters of  $A2/a$  phase with two sizes:  $5a \times 4b \times 10c$  (35; 35; 66 Å (6400 atoms)) and  $1a \times 1b \times 2c$  (7; 9; 12 Å (64 atoms)) matched the experiment well (Figs 10, *b* and 11, *b*). The atoms in  $5a \times 4b \times 10c$  clusters were displaced randomly from the initial positions with Gaussian's distribution dispersion equaled to 0.1 Å for the atoms of Ca, Si, O and to 0.12 Å for atoms Ti along the  $x, y, z$  axes of Cartesian coordinate system.

The theoretical scattering intensity  $I(s)$  was calculated by adding 0.5 of scattering intensity of the cluster with  $1a \times 1b \times 2c$  size and 0.5 of one of the cluster with  $5a \times 4b \times 10c$  size. The calculated  $R_p$  factor for scattering intensity  $I(s)$  of the mechanical mixtures was 6.9% (for the case of the disordered cluster of  $5a \times 4b \times 10c$ ) and was

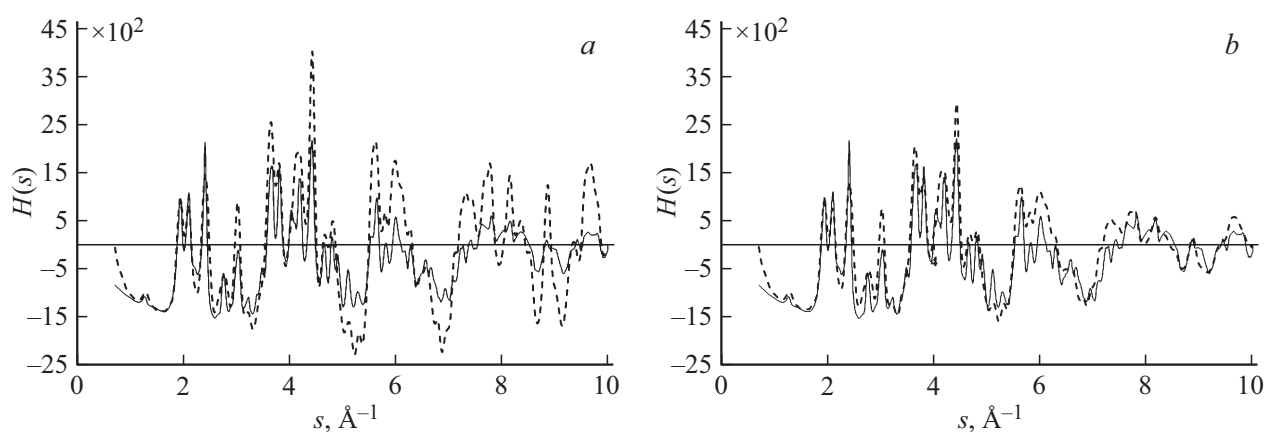


**Figure 11.** The  $s$ -weighted interference functions  $H(s)$ : experimental (solid line) and calculated (dashed line) for the mechanical mixtures of the clusters: a)  $1a \times 1b \times 2c$  and  $5a \times 4b \times 10c$ ; b)  $1a \times 1b \times 2c$  and the disordered one of  $5a \times 4b \times 10c$ .

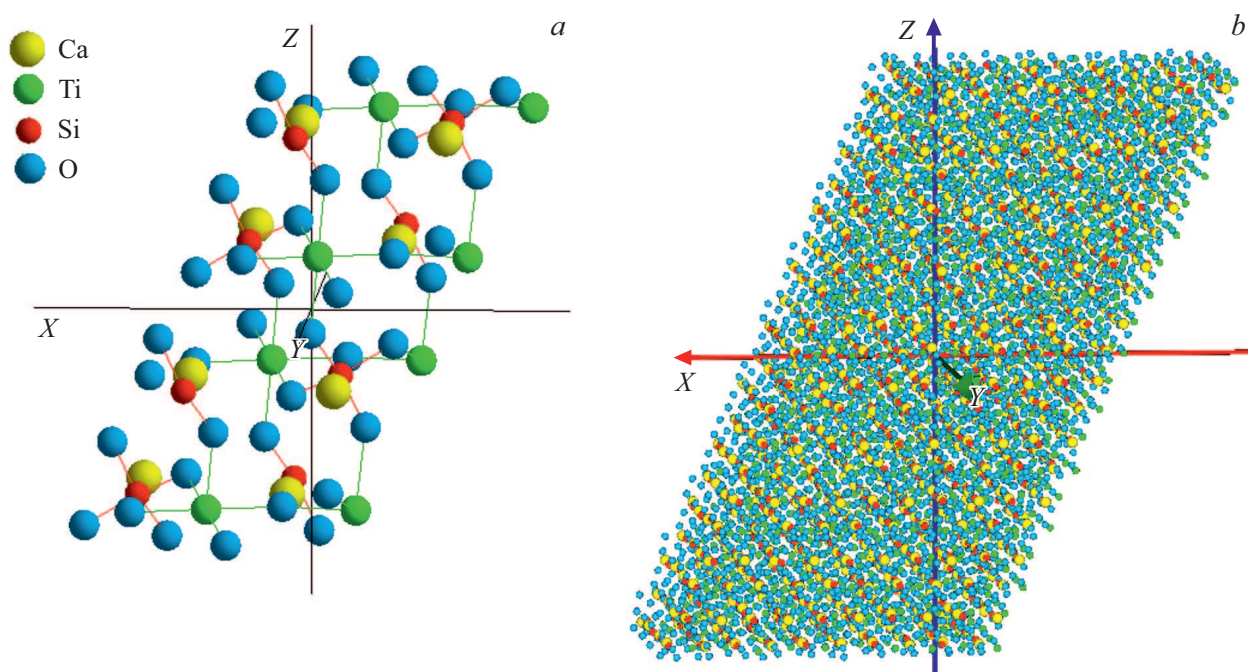


**Figure 12.** Nanosized clusters in the model of the mechanical mixture: a)  $1a \times 1b \times 2c$  (64 atoms) and b)  $5a \times 4b \times 10c$  (6400 atoms).

slightly higher than the Rietveld's  $R$ -factor for the data of the crystalline component of this sample (Fig. 1).

The first cluster consisted of 8 Ca atoms, 8 Si atoms, and 8 Ti atoms and 40 O atoms (Fig. 12, a). The second cluster consisted of 800 Ca atoms, 800 Si atoms, 800 Ti atoms and 4000 O atoms (Fig. 12, b). Calculated by Eq. (7), the concentrations of the model components were 50% for the cluster with  $5a \times 4b \times 10c$  size and 50% for the one with  $1a \times 1b \times 2c$  size.

Thus, the model of the mechanical mixture of the nanosized clusters of the  $A2/a$  phase with sizes of both  $1a \times 1b \times 2c$  and  $5a \times 4b \times 10c$  (the cations were displaced at random from the initial position in the latter cluster) described satisfactorily the structure of the titanite

mechanically activated for 30 min. in the mill with CF of 95 g (Pulverisette 7). Based on this model, it can be explained that the decrease of the coordination numbers of metal atoms was a consequence of a large number of boundary atoms (Table 7).

The comparison of the  $W(r)$  curves calculated from the experiment with one calculated for the model of mechanical mixture consisting of the clusters of both  $1a \times 1b \times 2c$  and  $5a \times 4b \times 10c$  shows that the order of atoms arrangement in the model is higher than in the experiment (Fig. 13).

In our model, the low number of oxygen atoms near Ti and the excessive number of those near Ca lead to the difference of far distances on the calculated for the model and experimental functions  $W(r)$ .

**Table 7.** The radii ( $\Delta r_{ij} = \pm 0.02 \text{ \AA}$ ) and blurring  $\sigma_{ij}$  ( $\Delta \sigma_{ij} = \pm 0.1 \text{ \AA}$ ) of the coordination spheres and the coordination numbers for the ground titanite sample for 30 min. in air (95 g) and the corresponding data calculated for the mechanical mixture of clusters of both  $1a \times 1b \times 2c$  and  $5a \times 4b \times 10c$

| Type of sphere | MA for 30 min. in air<br>(95 g) |                            |                                       | Mechanical mixture of clusters<br>$1a \times 1b \times 2c$ and $5a \times 4b \times 10c$ |                            |                    | $P2_1/a / A2/a$                       |                    |
|----------------|---------------------------------|----------------------------|---------------------------------------|--|----------------------------|--------------------|---------------------------------------|--------------------|
|                | $r_{ij}, \text{ \AA}$           | $\sigma_{ij}, \text{ \AA}$ | $\langle r_{ij} \rangle, \text{ \AA}$ | $r_{ij}, \text{ \AA}$  | $\sigma_{ij}, \text{ \AA}$ | $N_{ij},$<br>atoms | $\langle r_{ij} \rangle, \text{ \AA}$ | $N_{ij},$<br>atoms |
| Si–O(1)        | 1.64                            | 0.23                       | $3.93 \pm 0.04$                       | 1.65   | 0.17                       | $3.93 \pm 0.02$    | 1.64                                  | 4.00               |
| Ti–O(1)        | 1.95                            | 0.28                       | $4.50 \pm 0.05$                       | 1.955  | 0.10                       | $3.46 \pm 0.03$    | 1.88/1.94                             | 6.00               |
| Ca–O(1)        | 2.44                            | 0.30                       | $6.85 \pm 0.06$                       | 2.42   | 0.28                       | $7.70 \pm 0.08$    | 2.44                                  | 7.00               |
| O–O(1)         | 2.80                            | 0.20                       | $6.62 \pm 0.08$                       | 2.81   | 0.23                       | $6.03 \pm 0.16$    | 2.80                                  | 8.40               |
| Ca–Si(1)       | 3.06                            | 0.11                       | $0.94 \pm 0.05$                       | 3.06   | 0.01                       | $1.23 \pm 0.02$    | 3.06                                  | 1.00               |

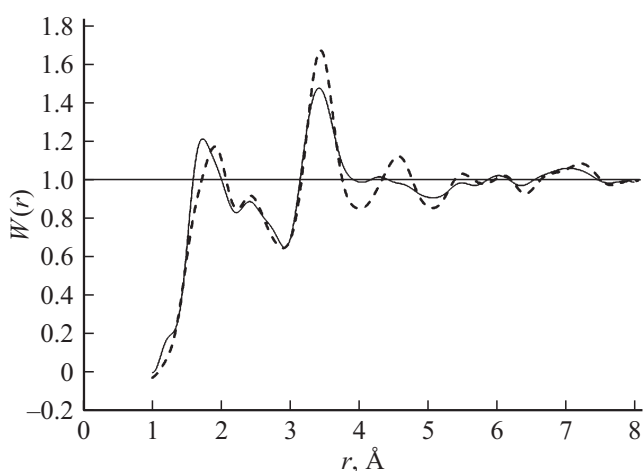


**Figure 13.** Pair correlation functions, solid line: calculated from the experiment, dashed line: calculated for the model of mechanical mixture consisting of the both clusters.

## Conclusion

Thus, mechanical activation of titanite in the mill with CF of 40 g in air and in  $\text{CO}_2$  atmosphere led to formation of amorphous and crystalline phases. The structure of the crystalline component corresponded to the  $P2_1/a$  phase with a partial change in the coordination of Ti and Ca atoms. This result was in good agreement with the data reported in [10–12].

The theoretical diffraction pattern calculated for mechanical mixture of the randomly disordered clusters with linear 21; 26; 46 Å sizes (2016 atoms) distorted in MD experiment and the clusters with 59.5; 78; 41 Å (12096 atoms) sizes were the closest to the experimental pattern of mechanically activated titanite for 30 min. in the mill with CF of 40 g.

The main difference of grinding in the mill with 95 g is the size reducing of clusters to 7; 9; 12 Å (64 atoms) and 35; 35; 66 Å (6400 atoms). Disordering of large clusters was by static displacement of atoms. The ratio between large and small clusters also changes. In the first case, the values of phase concentrations calculated for the model were 80 and

20%. In the second case, the contribution to the scattering intensity of large clusters increased and the values of phase concentrations were 50 and 50%. The models proposed in the paper are more suitable for describing the structure of studied materials.

## Acknowledgment

The authors are deeply grateful to A.M. Kalinkin, Doctor of Chemistry, Head of the Laboratory of minerals and silicate synthesis (ICTREMRM, Apatity) for providing the samples, and O.L. Dobrynina, PhD (Petrozavodsk State University) for providing language assistance.

## Conflicts of interest

The authors declare no conflicts of interest.

## Authors contribution

L.A. Aleshina: Conceptualization, methodology; O.V. Sidorova: Investigation, writing — review & editing, formal analysis; A.D. Fofanov: Software.

## References

- [1] L.G. Gerasimova, M.V. Maslova, E.S. Shchukina. Russ. J. Appl. Chem. **83**, 12, 2081 (2010). DOI: 10.1134/S1070427210120037
- [2] J. Maletaskić, B. Matović, N. Stanković, M. Prekajski-Djordjević, J. Luković, K. Yoshida, T. Yano. Energy Procedia **131**, 407 (2017). DOI: 10.1016/j.egypro.2017.09.457
- [3] E.W. Awini, B. Matovic, J. Maletaskic, V. Urbanovich, R. Kumar. Process. Appl. Ceram. **10**, 4, 295 (2016). DOI: 10.2298/PAC1604295A
- [4] A.M. Kalinkin, E.V. Kalinkina, T.N. Vasil'eva. Colloid J. **66**, 2, 160 (2004). DOI: 10.1023/B:COLL.0000023116.75353.f0
- [5] A. Amirjani, M. Hafezi, A. Zamanian, M. Yasae, N. Azuan Abu Osman. J. Adv. Mater. Process. **4**, 2, 56 (2016).
- [6] L.G. Gerasimova, V.V. Tyukavkina. Fundamental Res. **2**, 10, 2083 (2015). (in Russian).

- [7] T. Stoyanova-Lyubenova, F. Matteucci, A. Costa, M. Dondi, J. Carda. *Powder Technol.* **193**, 1, 1 (2009). DOI: 10.1016/j.powtec.2009.01.020
- [8] S. Cheng, D. Wei, Y. Zhou. *Appl. Surf. Sci.* **257**, 8, 3404 (2011). DOI: 10.1016/j.apsusc.2010.11.034
- [9] L. Nasdala, T. Stoyanova-Lyubenova, M. Gaft, M. Wildner, W. Diegor, C. Petautschnig, D. Talla, C. Lenz. *Chem. Erde* **74**, 3, 419 (2014). DOI: /10.1016/j.chemer.2014.04.004
- [10] T. Beirau. *Z. Kristallographie — Crystalline Mater.* **229**, 8, 543 (2014). DOI: 10.1515/zkri-2014-1745
- [11] T. Beirau, U. Bismayer, B. Mihailova, C. Paulmann, L. Groat. *Phase Transitions* **83**, 9, 694 (2010). DOI: /10.1080/01411594.2010.502875
- [12] T. Beirau. PhD Thesis, Fachbereich Geowissenschaften der Universität Hamburg, Hamburg (2012). 102 p.
- [13] S.J.L. Billinge. *Phil. Trans. R. Soc. A* **377**, 2147, 20180413 (2019). DOI: 10.1098/rsta.2018.0413
- [14] O.V. Sidorova, L.A. Aleshina, D.S. Krupyanskiy. *Int. J. Mineral Proc.* **169**, 119 (2017). DOI: 10.1016/j.minpro.2017.11.001
- [15] E.G. Avvakumov. *Mekhanicheskie metody aktivatsii khimicheskikh protsessov (Mechanical Activation of Chemical Processes)*, Nauka, Novosibirsk (1989). 306 p. (in Russian)
- [16] V.B. Zlokazov, V.V. Chernyshev. *J. Appl. Crystallogr.* **25**, Part 3, 447 (1992). DOI: 10.4028/www.scientific.net/MSF.79-82.283
- [17] O. Borgen, C. Finbak. *Acta Chem. Scand.* **8**, 829 (1954). DOI: 10.3891/acta.chem.scand.08-0829
- [18] B.E. Warren. *X-ray diffraction*. Addison-Wesley, Reading, MA (1969). 381 p.
- [19] R.L. Mozzi, B.E. Warren. *J. Appl. Cryst.* **2**, 4, 164 (1969). DOI: 10.1107/S0021889869006868
- [20] R.L. Mozzi, B.E. Warren. *J. Appl. Cryst.* **3**, 4, 251 (1970). DOI: 10.1107/S0021889870006143
- [21] B.E. Warren. *Chem. Rev.* **26**, 2, 237 (1940). DOI: 10.1021/cr60084a007
- [22] L.A. Aleshina, V.P. Malinenko, A.D. Phouphanov, N.M. Jakovleva. *J. Non-Cryst. Solids* **87**, 3, 350 (1986). DOI: 10.1016/S0022-3093(86)80008-4
- [23] L.A. Aleshina, A.D. Fofanov. *X-ray Structural Analysis of Amorphous Materials*. PetrSU, Petrozavodsk (1987). 85 p.
- [24] N.S. Skorikova, D.V. Loginov, O.V. Sidorova, A.D. Fofanov, E.F. Kudina. *Glass Phys. Chem.* **44**, 6, 575 (2018). DOI: 10.1134/S1087659618060202
- [25] G.E. Forsythe, M.A. Malcolm, C.B. Moler. *Computer Methods for Mathematical Computations*. Englewood Cliffs: Prentice Hall (1977). 259 p.
- [26] C.L. Lawson, R.J. Hanson. *Solving Least Squares Problems*. Philadelphia: SIAM (1995). 337 p.
- [27] D.V. Lobov, A.D. Fofanov, R.N. Osaulenko, A.M. Kalinkin. *Electron. J. „Investigated in Russia“* **085**, 889 (2005). Access mode: <http://zhurnal.ape.relarn.ru/articles/2005/085.pdf>
- [28] A.D. Fofanov. *The structure and short-range order in the oxygen- and carbon-containing systems with special properties*. PhD Thesis, Moscow State University (1998). 343 p.
- [29] P. Scardi, L. Gelisio. *Sci. Rep.* **6**, 22221 (2016). DOI: 10.1038/srep22221
- [30] M. Rudolph, M. Motylenko, D. Rafaja. *IUCrJ* **6**, Part 1, 116 (2019). DOI: 10.1107/S2052252518015786
- [31] V.P. Pakharukova, D.A. Yatsenko, E.Y. Gerasimov, A.S. Shalygina, O.N. Martyanova, S.V. Tsybulya. *J. Solid State Chem.* **246**, 284 (2017). DOI: 10.1016/j.jssc.2016.11.032
- [32] M.E. Prokhoriskii, A.D. Fofanov, L.A. Aleshina, E.A. Nikitina. *Crystallogr. Rep.* **49**, 4, 631 (2004). DOI: 10.1134/1.1780628
- [33] V.S. Urusov, N.N. Eremin. *Computer modeling of structures and properties of crystals — advancements and opportunities*. *Problemy Kristallografi* **5**, 228, GEOS, Moscow (1999). (in Russian)
- [34] T.S. Bush, J.D. Gale, C.R.A. Catlow, P.D. Battle. *J. Mater. Chem.* **4**, 6, 831 (1994). DOI: 10.1039/jm9940401765
- [35] N.N. Eremin, V.S. Urusov, V.S. Rusakov, O.V. Yakubovich. *Crystallogr. Rep.* **47**, 5, 759 (2002). DOI: 10.1134/1.1509390
- [36] G.K. Williamson, W.H. Hall. *Acta Metallurgica* **1**, 1, 22 (1953). DOI: 10.1016/0001-6160(53)90006-6
- [37] V.I. Iveronova, G.P. Revkevich. *The theory of X-ray scattering*. Moscow State University Press, Moscow (1978). 246 p.
- [38] D. Balzar. *Res. Natl. Inst. Stand. Technol.* **98**, 3, 321 (1993). DOI: 10.6028/jres.098.026
- [39] W. Ruland. *Acta Crystallogr.* **14**, 11, 1180 (1961). DOI: 10.1107/S0365110X61003429
- [40] M. Kunz, T. Arlt, J. Stolz. *Am. Mineral.* **85**, 10, 1465 (2000). DOI: 10.2138/am-2000-1016
- [41] M. Kunz, D. Xirouchakis, D.H. Lindsley, D. Haeusermann. *Am. Mineral.* **81**, 11–12, 1527 (1996). DOI: 10.2138/am-1996-11-1225
- [42] J.A. Speer, G.V. Gibbs. *Am. Mineral.* **61**, 3–4, 238 (1976).
- [43] M. Taylor, G.E. Brown. *Am. Mineral.* **61**, 5–6, 435 (1976).
- [44] O.V. Sidorova, L.A. Aleshina, A.M. Kalinin, E.V. Kalinkina. *Petrozavodsk State University Proceed., Ser. „Natural. Engg Sci.“* **4**, 125, 112 (2012).
- [45] B.D. Cullity. *Elements of X-ray diffractions*. Addison-Wesley, Reading, MA (1956). 555 p.